## SUPPLEMENTAL LEGENDS

### Figure S1

**Whole cell images for dynein/dynactin colocalization with incoming adenovirus.** Whole cell images for dynein/dynactin colocalization with incoming adenovirus for enlarged regions shown in Fig 1A-C. In the case of p150$^{Glued}$, the particular cell chosen for enlargement was at the edge of the field of view and, therefore, not entirely visible.

### Figure S2

**Characterization of viral polypeptides. (A)** Colocalization of penton base with Ad5 particles in infected cells. HeLa cells infected with Cy3-Ad5 (red) were fixed 60 min p.i. and stained with DAPI (blue) and with antibody against the penton base capsid protein (green). Penton base staining was clearly visible on capsids at the nucleus. The boxed region is enlarged (right) to show that some, but not all, virus particles are positive for penton base at this stage of infection. (**B**) Hexon runs as the native trimer on SDS gels, visible when unboiled transfected COS-7 lysates are analyzed by immunoblotting. (**C**) Similarly, penton base behaves as its native pentamer, although monomer is also visible in unboiled samples. (**D**) Subcellular localization of overexpressed viral polypeptides imaged using antibodies against epitope tags, GFP fusion or anti-hexon antibody (green). Each of the proteins localized within cells as previously reported, with protein V present in nucleoli, protein VII in the nucleus and nucleoli, protein X in nucleoli with cytoplasmic background, penton base in the nucleus, and hexon in the cytoplasm. DAPI staining is in blue. (**E**) Protein VII was present only in the nuclear fraction of cell lysates, which was devoid of dynein. (Scale bars = 5 μm)

**Figure S3**

**Immunoisolation of hexon.** (**A**) Coomassie blue stained gel of immunoprecipitations performed using monoclonal anti-hexon and anti-fiber antibodies from late-stage infected 293A cell lysate. The hexon beads were washed, resuspended at either pH 7.4 ($P_1$) or pH 4.4 ($P_2$), and then subjected to SDS gel electrophoresis. The pellets show hexon as the major band (white star), with the antibody heavy and light chains as secondary bands (white arrow and arrowhead, respectively). Immunoprecipitated with anti-fiber monoclonal antibody was performed in the same manner, and yielded fiber as the major band (black star), which is clearly depleted in the hexon immunoprecipitates. (**B**) Western blot of the same samples. (**C**) Antibody specificity of anti-hexon (anti-hex) and anti-dynein IC (anti-IC) by Western blot of COS-7 cell lysate. Coomassie blue stained membrane shown.

**Figure S4**

**Dynein HC RNAi interferes with Ad5 redistribution.**

(**A**) Western blot of dynein HC knockdown by RNAi. A549 cells were transfected with a cDNA encoding GFP and a shRNAi corresponding to sequence within the rat cytoplasmic dynein HC. The HC signal was reduced to 93.8% (after 24 hrs), 26.6% (48 hrs), and 19.6% (72 hrs). Tubulin is included as loading control. (**B**) Effect of HC RNAi on adenovirus distribution. Cells expressing the HC RNAi construct for 0-3 days were infected with Alexa-Ad5 and fixed and immunostained at 60 min p.i. Adenovirus particles were found increasingly dispersed throughout the cytoplasm with decreasing HC

levels. (**C**) The Golgi apparatus immunostained using anti-GM130 antibody was similarly dispersed over a comparable time period in cells subjected to HC RNAi. Ad5 is shown in red and DAPI in blue. Scale bar = 10 μm. (**D)** Quantification for **B.** All differences to the control case are statistically significant ($P<0.01$; t-test). **(E)** Quantification for **C**.

**Figure S5**

**Expression of dominant negative dynein and dynactin constructs interferes with Ad5 redistribution.**

(**A**) COS-7 and (**B**) A549 cells were transfected with dynein or dynactin dominant negative constructs (green) and infected with Alexa -Ad5 (red). Cells were fixed and stained after 60 min. p.i. Ad5 no longer accumulated at the nucleus under the conditions examined. Scale bar = 5 μm. (**C**) Quantification of the effect of the dominant negative dynein and dynactin constructs on Ad5 redistribution. All values are statistically significant compared to the control case ($P < 0.01$; t-test).

**Figure S6**

**Purification of rat cytoplasmic dynein and hexon.**

(**A**) Coomassie blue-stained SDS electrophoretic gel of the final sucrose gradient step of rat brain cytoplasmic dynein purification (Paschal and Vallee, 1987). The dynein HC, IC, LIC1, and LIC2 peak in fractions 2–4, which were used for further experiments. Dynactin is not detected in the dynein peak. Actin commonly spreads throughout the gradient as seen here. (**B**) Coomassie blue-stained SDS electrophoretic gel of MonoQ

hexon. We observe a ~55 kDa contaminant in the hexon MonoQ peak, which, however, is absent in our hexon pull-downs.

**Figure S7**

**Selection of valid adenovirus tracks.**

(**A**) Virus tracks (blue) from a representative 1 min movie were overlaid onto bright field images of infected COS-7 cells to illustrate selection of virus particles (red) for further analysis. 'All tracks' (left panel) shows all particles observed for more than 100 frames during the course of the movie (blue). The few unmarked virus particles either came into view by the end of the recording period or exhibited non-Gaussian behavior were not scored. To identify directional tracks, (middle panel) diffusive particles were eliminated. These were defined by a total displacement in any direction < 1 μm or a net displacement below $\sqrt{4Dt}$, where $D=7.7*10^{-1}$ $\mu m^2$/sec. Thus, we imposed a total travel cut off which scaled as a square root of track time duration and only considered tracks which exceeded this cut off. Directionally moving particles (right panel) were then selected as those exhibiting translocations of $RT_1 > 2$ (see Methods for definitions). To define the direction of movement, the ratio of displacements was determined along and perpendicular to a line drawn between the center of a given track and the position of the centrosome. Only those particles for which $RT_2 > MAX(1.5, RT_1/10)$ were assigned a direction (plus or minus) and considered valid for final analysis. In other words, tracks were considered valid for our analysis if they showed significant motility, were linearly extended, and the direction of this extension roughly aligned with the direction to/from

the MTOC. (**B**) Lysosomal motility was not altered in COS-7 cells injected with anti-hexon antibody.

**Supplemental Movie 1**

**Adenovirus transport in uninjected COS-7 cell.**

COS-7 cell was infected with Alexa-Ad5 virus and imaged continuously for 1 min at 25 min p.i., replayed at 2x real time.

**Supplemental Movie 2**

**Adenovirus transport in anti-IgG injected cell.**

COS-7 cell was injected with anti-IgG 10 min prior to infection with Alexa-Ad5 virus. This movie was acquired continuously for 1 min at 35 min p.i., replayed at 2x real time.

**Supplemental Movie 3**

**Adenovirus transport in anti-hexon antibody-injected cell.**

COS-7 cell was injected with anti-hexon antibody 10 min prior to infection with Alexa-Ad5 virus. This movie was acquired at 62 min p.i. and imaging was as in Supplemental Movie 2.

**Supplemental Movie 4**

**Adenovirus transport in anti-dynein-IC antibody-injected cell.**

COS-7 cell was injected with anti-dynein IC antibody 10 min prior to infection with Alexa-Ad5 virus. This movie was acquired at 44 min p.i. and imaging was as in Supplemental Movie 2.

## SUPPLEMENTAL MATERIALS AND METHODS

### Motility analysis

A custom-tracking algorithm was used to extract the position of virus particles as a function of time. First, background fluorescence was estimated by applying a broad 2-D Savitsky-Golay smoothing filter to each frame. After subtracting this background intensity, all fluorescent particles within the cell outlines were fit to 2-D Gaussian profiles. Because virus particles are ~100 nm in diameter, their fluorescence signal can be treated as coming from a diffraction limited point source. This is an Airy function (Juskaitis, 2006) which is well approximated by a Gaussian shape near its peak (Carter et al., 2008; Cheezum et al., 2001). Positions of each particle were obtained from the Gaussian fits. Trajectories were reconstructed by matching particle locations based on their displacements between frames and confidence levels of the Gaussian fits. The details of the tracking algorithm will be published elsewhere.

To select only tracks corresponding to fast long-distance transport we have discarded tracks whose total displacement in any direction for the duration of the recording did not exceed 1 μm or whose displacement was below $\sqrt{4Dt}$ where $D=7.7*10^{-1}$ $\mu m^2$/sec. The latter independently estimated restriction is in good agreement with the upper range for diffusion coefficients reported by (Helmuth et al., 2007).

We further set up automated heuristic criteria to identify particles for which plus and minus directions of motion were clearly defined. To do this we first selected highly elongated tracks – a necessary attribute of motion along a single microtubule. We found

the direction of maximum displacement for each track and computed the ratios of displacement along this direction and along the orthogonal direction ($RT_1$). Tracks with $RT_1 < 2$ were excluded from analysis. We then selected for tracks moving mostly towards or away from the centrosome. Direction between the geometric centre of a track and centrosome were estimated for each particle and ratios of displacement along and perpendicular to these directions were computed ($RT_2$). Only tracks with $RT_2 > MAX(1.5, RT_1/10)$ were used for analysis. An example of the results of our automated track discrimination can be seen in supplemental figure S7. Tracks less than 100 frames long were not used in our analysis because they were not long enough to distinguish between different types of motion. Tracks which satisfied the above requirements were analyzed as previously described (Petrov et al., 2007). In particular, all tracks were automatically parsed into segments of constant velocity. Consecutive segments of motion in the same direction were pooled into "runs". Net velocities for each run were estimated by dividing the run length by its temporal duration.

**Antibodies**

Antibodies used included mouse monoclonal anti-hexon (Novocastra), anti-dynein IC (Chemicon), anti-p150$^{Glued}$, anti-GM130 (BD Biosciences), anti-clathrin, and anti-EEA-1 (BD Transduction Labs), rabbit polyclonal anti-dynein HC (Mikami et al., 2002; Roghi and Allan, 1999), anti-dynein IC (Vaughan and Vallee, 1995), pan anti-dynein LIC and anti-LIC2 (Tynan et al., 2000a; Tynan et al., 2000b), anti-dynein LC8 and anti-LIS1 (Santa Cruz Biotechnology, Inc), anti-Arp1 (Garces et al., 1999), anti-NudE/NudEL (Stehman et al., 2007), anti-NudC (Aumais et al., 2001), anti-ZW10 (Starr et al., 1998), anti-adenovirus (Abcam), and anti-GFP (Invitrogen), anti-penton base (Karayan et al.,

1997), anti-Giantin, anti-myc (Covance), and chicken anti-LIC1, which will be described elsewhere(Tan and Vallee, unpublished). Each antibody used for colocalization experiments tested negative for cross-reactivity with purified adenovirus by Western blotting (data not shown).

**Plasmids, RNAi, transfections and infections**

Plasmids encoding hexon-myc and 100K-HA (Wodrich et al., 2003) were obtained from L. Gerace (Scripps Research Institute, La Jolla, CA). Those encoding protein VII-GFP, protein V-GFP and protein X-GFP (Lee et al., 2003; Lee et al., 2004; Matthews and Russell, 1998) were from D. Matthews (Bristol University, UK) and penton base in pGmAc 115T (Karayan et al., 1994; Royer et al., 1992) from P. Boulanger (Institut de Biologie, Montpellier, France). Penton base, with a HA tag introduced, was amplified by PCR and inserted into the *EcoRI* and *NotI* sites of pcDNA3.1 (Invitrogen Corp.). The 100K coding region was amplified by PCR and introduced into the *EcoRI* and *BamHI* sites of pEGFP-N1 (Clontech). p50-myc (dynamitin), LIS1N-GFP, and NudE N189-GFP plasmids were described previously (Echeverri et al., 1996; Faulkner et al., 2000; Stehman et al., 2007) as were pCMV-CC1 (Quintyne et al., 1999), pRNAT-DHC RNAi (Tsai et al., 2007), a "headless" dynein HC tail fragment C1140 (Varma et al., 2008), IC2C-GFP (Towns et al., 2009), GFP-LIC1, -LIC2 (will be published elsewhere), and VSVG-LC8, HA-RP3, HA-TcTex1 (Tai et al, 2002). ΔNp150$^{Glued}$ was designed on the basis of a previous report (Kim et al., 2007). A fragment of rat p150$^{Glued}$ cDNA (a.a. 212 -1325) lacking the N-terminal microtubule binding domain was amplified by PCR and

cloned in frame with GFP into the restriction sites XhoI and SacII in the pEGFP-C1 vector (Clontech). ZW10 siRNA was performed as described (Varma et al., 2006).

**SUPPLEMENTAL REFERENCES**


Aumais, J. P., Tunstead, J. R., McNeil, R. S., Schaar, B. T., McConnell, S. K., Lin, S. H., Clark, G. D., and Yu-Lee, L. Y. (2001). NudC associates with Lis1 and the dynein motor at the leading pole of neurons. J Neurosci *21*, RC187.

Carter, B. C., Vershinin, M., and Gross, S. P. (2008). A comparison of step-detection methods: how well can you do? Biophys J *94*, 306-319.

Cheezum, M. K., Walker, W. F., and Guilford, W. H. (2001). Quantitative comparison of algorithms for tracking single fluorescent particles. Biophys J *81*, 2378-2388.

Echeverri, C. J., Paschal, B. M., Vaughan, K. T., and Vallee, R. B. (1996). Molecular characterization of the 50kD subunit of dynactin reveals function for the complex in chromosome alignment and spindle organization during mitosis. J Cell Biol *132*, 617-633.

Faulkner, N. E., Dujardin, D. L., Tai, C. Y., Vaughan, K. T., O'Connell, C. B., Wang, Y., and Vallee, R. B. (2000). A role for the lissencephaly gene LIS1 in mitosis and cytoplasmic dynein function. Nat Cell Biol *2*, 784-791.

Garces, J. A., Clark, I. B., Meyer, D. I., and Vallee, R. B. (1999). Interaction of the p62 subunit of dynactin with Arp1 and the cortical actin cytoskeleton. Curr Biol *9*, 1497-1500.

Helmuth, J. A., Burckhardt, C. J., Koumoutsakos, P., Greber, U. F., and Sbalzarini, I. F. (2007). A novel supervised trajectory segmentation algorithm identifies distinct types of human adenovirus motion in host cells. J Struct Biol *159*, 347-358.

Juskaitis, R. (2006). Measuring the real point spread function of high numerical aperture microscope objective lenses, In The Handbook of Confocal Microscopy (Springer).

Karayan, L., Gay, B., Gerfaux, J., and Boulanger, P. A. (1994). Oligomerization of recombinant penton base of adenovirus type 2 and its assembly with fiber in baculovirus-infected cells. Virology *202*, 782-795.

Karayan, L., Hong, S. S., Gay, B., Tournier, J., d'Angeac, A. D., and Boulanger, P. (1997). Structural and functional determinants in adenovirus type 2 penton base recombinant protein. J Virol *71*, 8678-8689.

Kim, H., Ling, S. C., Rogers, G. C., Kural, C., Selvin, P. R., Rogers, S. L., and Gelfand, V. I. (2007). Microtubule binding by dynactin is required for microtubule organization but not cargo transport. J Cell Biol *176*, 641-651.

Lee, T. W., Blair, G. E., and Matthews, D. A. (2003). Adenovirus core protein VII contains distinct sequences that mediate targeting to the nucleus and nucleolus, and colocalization with human chromosomes. J Gen Virol *84*, 3423-3428.

Lee, T. W., Lawrence, F. J., Dauksaite, V., Akusjarvi, G., Blair, G. E., and Matthews, D. A. (2004). Precursor of human adenovirus core polypeptide Mu targets the nucleolus and modulates the expression of E2 proteins. J Gen Virol *85*, 185-196.

Matthews, D. A., and Russell, W. C. (1998). Adenovirus core protein V is delivered by the invading virus to the nucleus of the infected cell and later in infection is associated with nucleoli. J Gen Virol *79 (Pt 7)*, 1671-1675.

Mikami, A., Tynan, S. H., Hama, T., Luby-Phelps, K., Saito, T., Crandall, J. E., Besharse, J. C., and Vallee, R. B. (2002). Molecular structure of cytoplasmic dynein 2 and its distribution in neuronal and ciliated cells. J Cell Sci *115*, 4801-4808.

Paschal, B. M., and Vallee, R. B. (1987). Retrograde transport by the microtubule associated protein MAP 1C. Nature *330*, 181-183.

Petrov, D. Y., Mallik, R., Shubeita, G. T., Vershinin, M., Gross, S. P., and Yu, C. C. (2007). Studying molecular motor-based cargo transport: what is real and what is noise? Biophys J *92*, 2953-2963.

Quintyne, N. J., Gill, S. R., Eckley, D. M., Crego, C. L., Compton, D. A., and Schroer, T. A. (1999). Dynactin is required for microtubule anchoring at centrosomes. J Cell Biol *147*, 321-334.

Roghi, C., and Allan, V. J. (1999). Dynamic association of cytoplasmic dynein heavy chain 1a with the Golgi apparatus and intermediate compartment. J Cell Sci *112 (Pt 24)*, 4673-4685.

Royer, M., Hong, S. S., Gay, B., Cerutti, M., and Boulanger, P. (1992). Expression and extracellular release of human immunodeficiency virus type 1 Gag precursors by recombinant baculovirus-infected cells. J Virol *66*, 3230-3235.

Starr, D. A., Williams, B. C., Hays, T. S., and Goldberg, M. L. (1998). ZW10 helps recruit dynactin and dynein to the kinetochore. J Cell Biol *142*, 763-774.

Stehman, S. A., Chen, Y., McKenney, R. J., and Vallee, R. B. (2007). NudE and NudEL are required for mitotic progression and are involved in dynein recruitment to kinetochores. J Cell Biol *178*, 583-594.

Tynan, S. H., Gee, M. A., and Vallee, R. B. (2000a). Distinct but overlapping sites within the cytoplasmic dynein heavy chain for dimerization and for intermediate chain and light intermediate chain binding. J Biol Chem *275*, 32769-32774.

Tynan, S. H., Purohit, A., Doxsey, S. J., and Vallee, R. B. (2000b). Light intermediate chain 1 defines a functional subfraction of cytoplasmic dynein which binds to pericentrin. J Biol Chem *275*, 32763-32768.

Varma, D., Dujardin, D. L., Stehman, S. A., and Vallee, R. B. (2006). Role of the kinetochore/cell cycle checkpoint protein ZW10 in interphase cytoplasmic dynein function. J Cell Biol *172*, 655-662.

Vaughan, K. T., and Vallee, R. B. (1995). Cytoplasmic dynein binds dynactin through a direct interaction between the intermediate chains and p150 $^{Glued}$. J Cell Biol *131*, 1507-1516.

Wodrich, H., Guan, T., Cingolani, G., Von Seggern, D., Nemerow, G., and Gerace, L. (2003). Switch from capsid protein import to adenovirus assembly by cleavage of nuclear transport signals. Embo J *22*, 6245-6255.

[F] Supplemental Figure1

# Figure S1

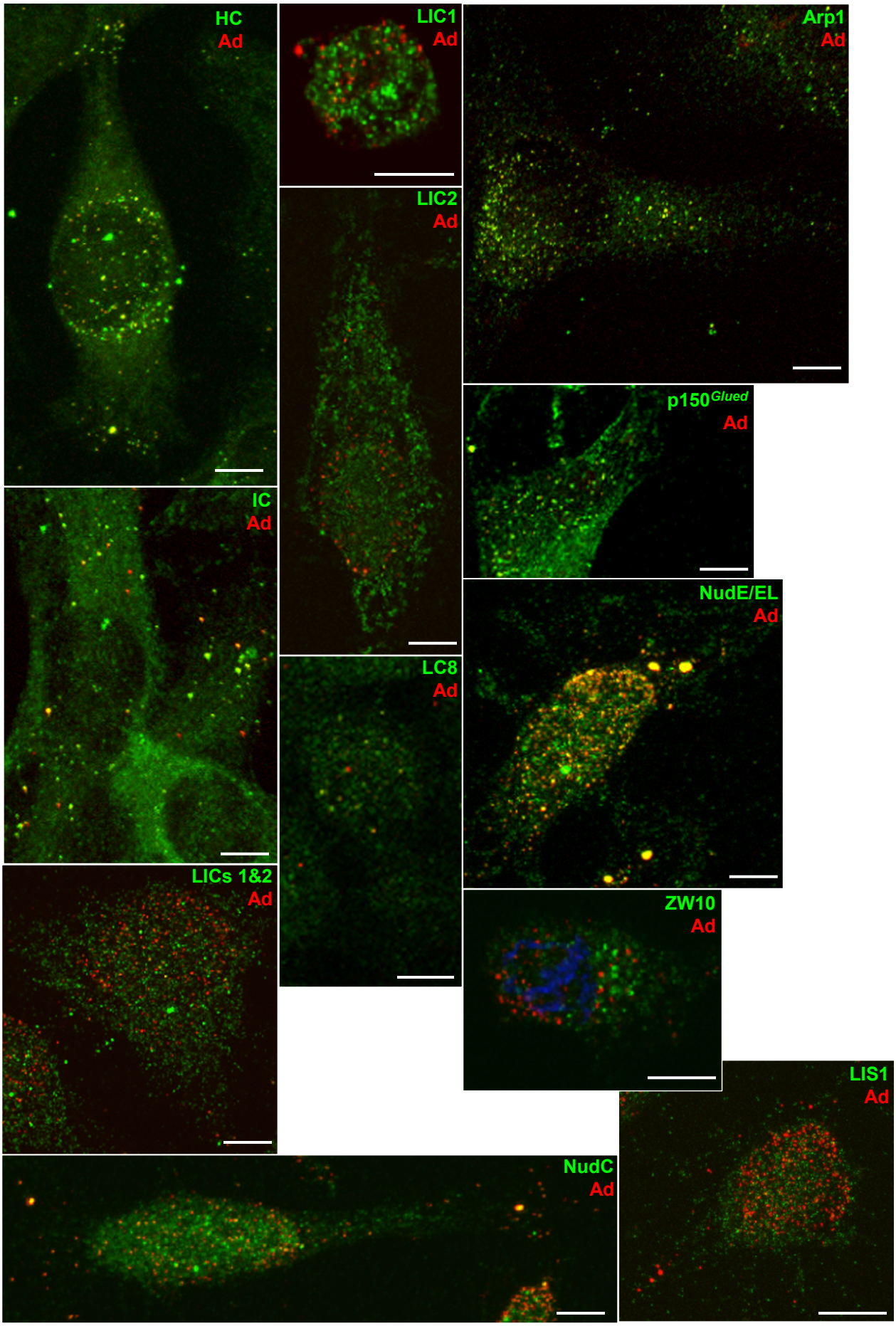

# Figure S2

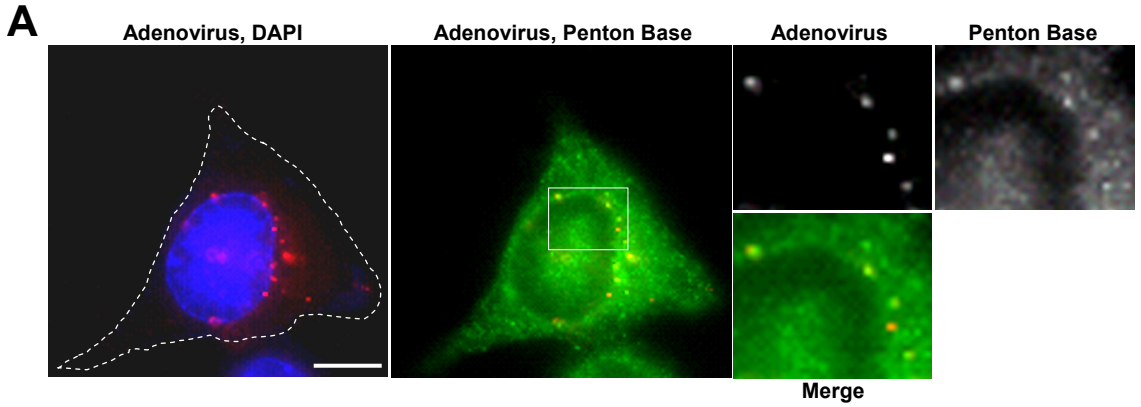
A
Adenovirus, DAPI
Adenovirus, Penton Base
Adenovirus
Penton Base
Merge
B
not
boil boil
Hexon-myc trimer (360 kD)
Hexon-myc monomer (120 kD)
C
not
boil boil
PB-HA pentamer (425 kD)
PB-HA monomer (85 kD)
D
Protein VII-GFP
Hexon-myc
Protein V-GFP
Penton Base-HA
Protein X-GFP
E
Nuclear Prep
S
P
IC (74 kD)
pVII-GFP (45 kD)

[F] Supplemental Figure3

# Figure S3

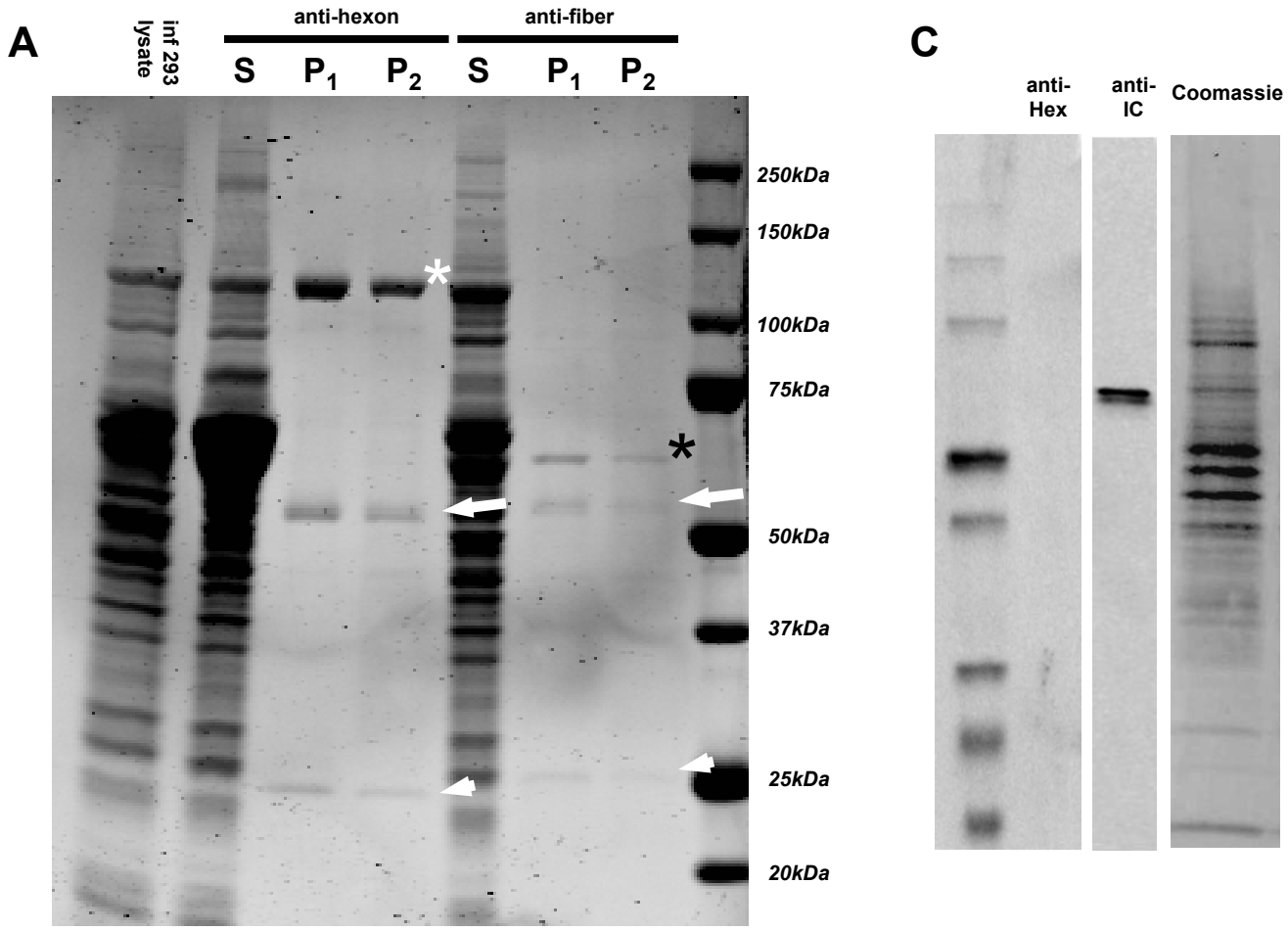

[F] Supplemental Figure4

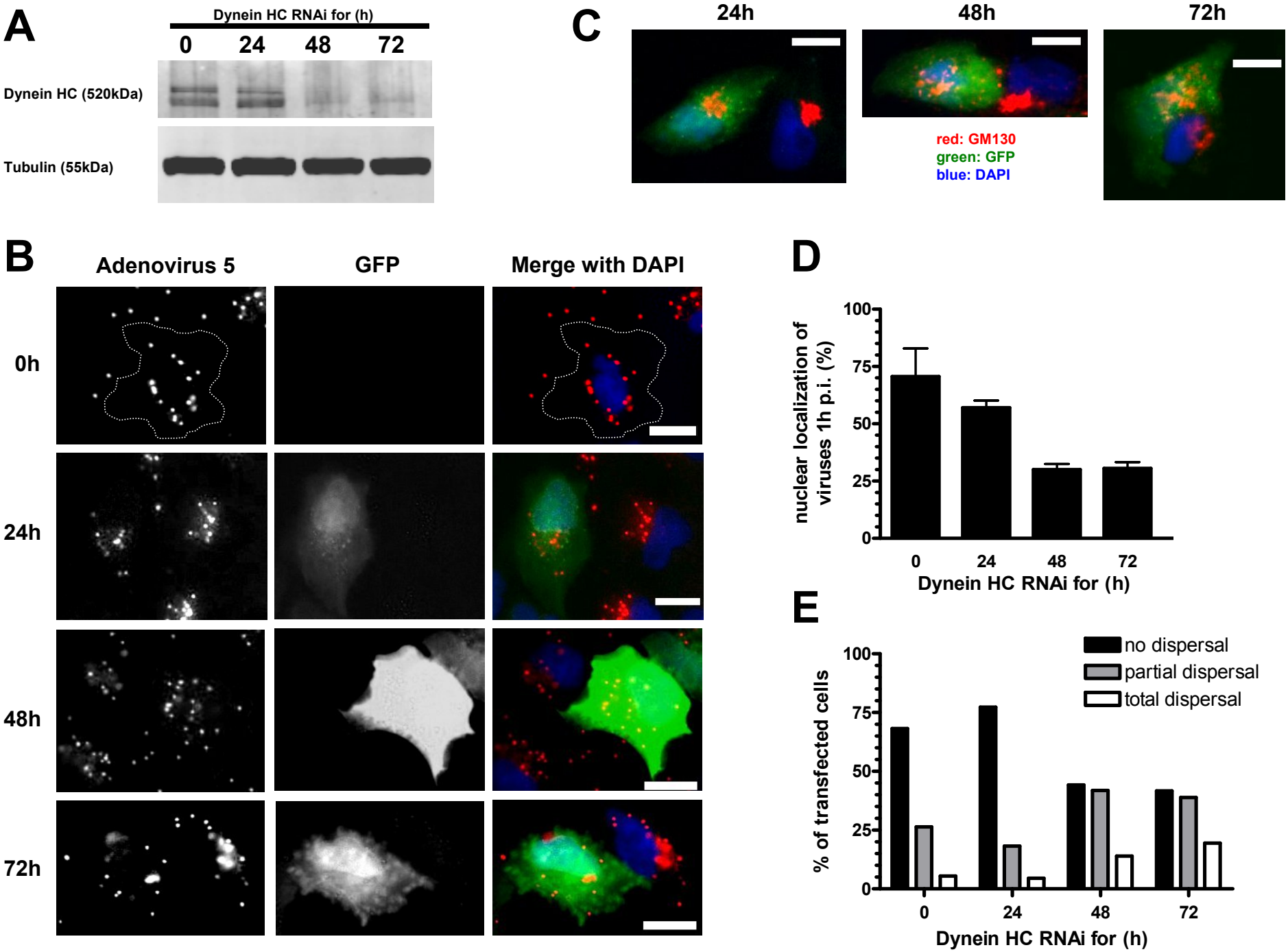

# Figure S5

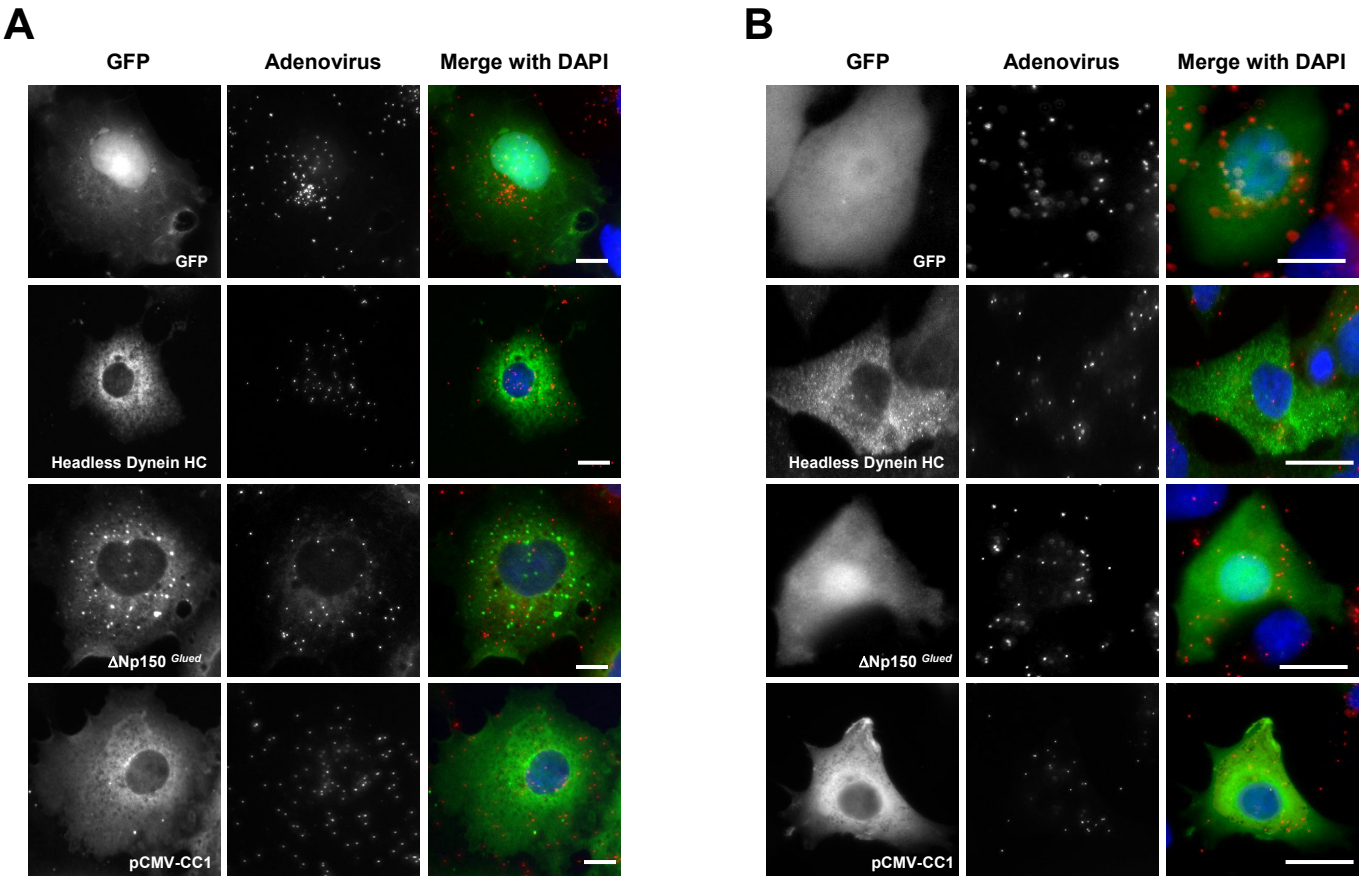
A
GFP
Adenovirus
Merge with DAPI
GFP
Headless Dynein HC
ΔNp150 Glued
pCMV-CC1
B
GFP
Adenovirus
Merge with DAPI
GFP
Headless Dynein HC
ΔNp150 Glued
pCMV-CC1

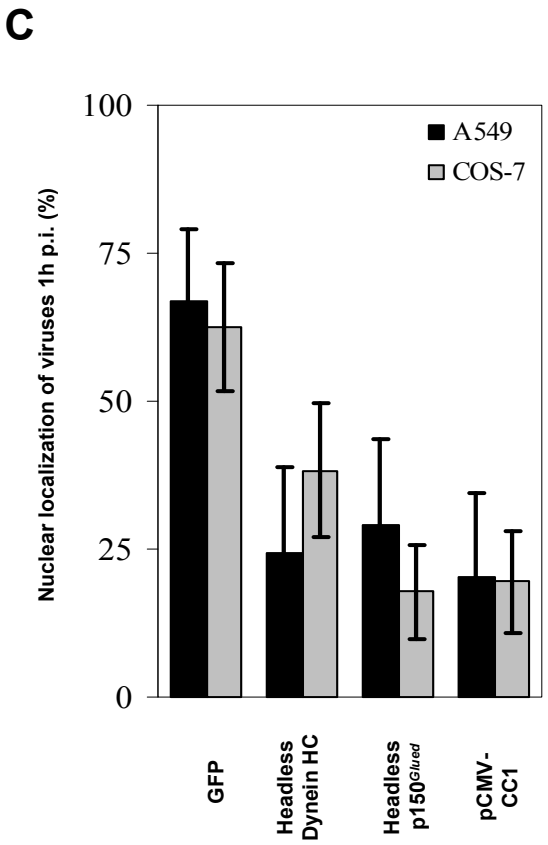
C
Nuclear localization of viruses 1h p.i. (%)
100
75
50
25
0
A549
COS-7
GFP
Headless Dynein HC
Headless p150Glued
pCMV-CC1

# Figure S6

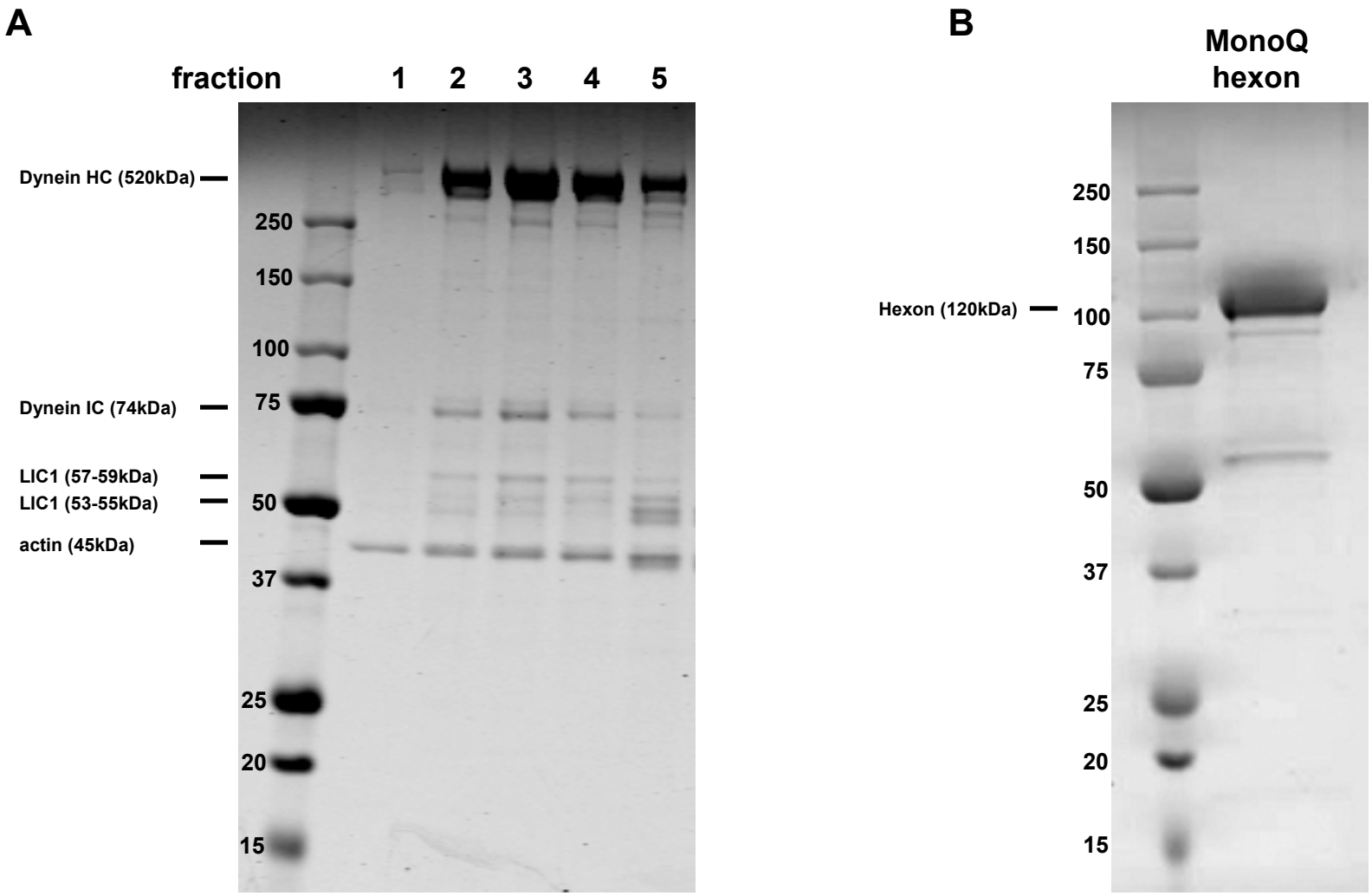
A
fraction
1
2
3
4
5
Dynein HC (520kDa)
Dynein IC (74kDa)
LIC1 (57-59kDa)
LIC1 (53-55kDa)
actin (45kDa)
250
150
100
75
50
37
25
20
15
B
MonoQ
hexon
Hexon (120kDa)
250
150
100
75
50
37
25
20
15

[F] Supplemental Figure7

# Figure S7

## A

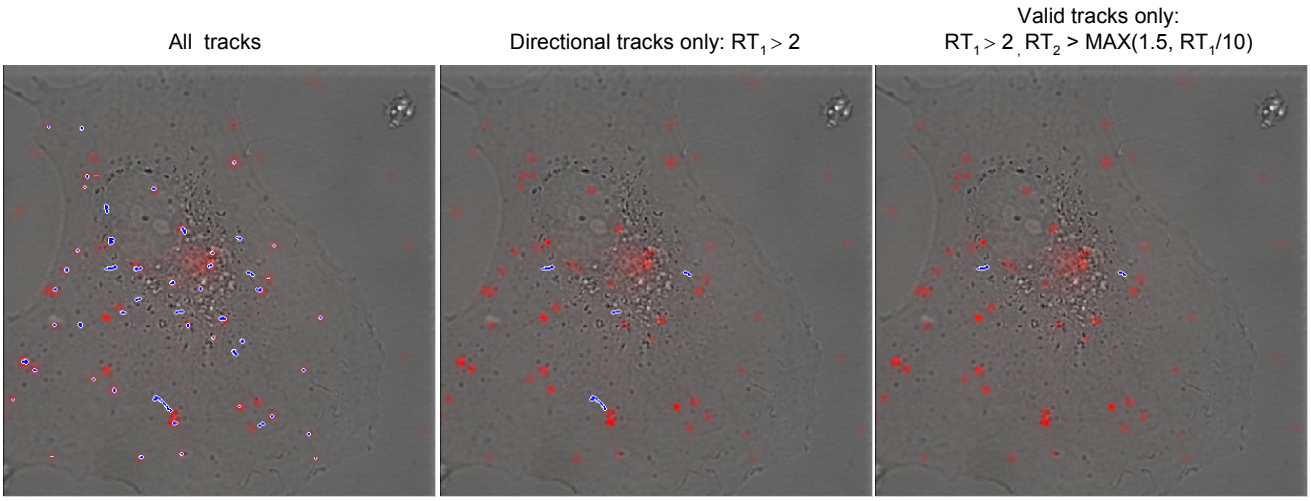


## B